SCIENCE CHINA
Earth Sciences

• RESEARCH PAPER •

June 2014 Vol.57 No.6: 1278–1292
doi: 10.1007/s11430-013-4798-8

Improvement of snow depth retrieval for FY3B-MWRI in China

JIANG LingMei[1*], WANG Pei[1], ZHANG LiXin[1], YANG Hu[2] & YANG JunTao[1]

[1] *State Key Laboratory of Remote Sensing Science, School of Geography, Beijing Normal University, Beijing 100875, China;*
[2] *National Satellite Meteorological Center, China Meteorological Administration, Beijing 100081, China*

Received February 22, 2013; accepted July 25, 2013; published online February 12, 2014

The primary objective of this work is to develop an operational snow depth retrieval algorithm for the FengYun3B Microwave Radiation Imager (FY3B-MWRI) in China. Based on 7-year (2002–2009) observations of brightness temperature by the Advanced Microwave Scanning Radiometer-EOS (AMSR-E) and snow depth from Chinese meteorological stations, we develop a semi-empirical snow depth retrieval algorithm. When its land cover fraction is larger than 85%, we regard a pixel as pure at the satellite passive microwave remote-sensing scale. A 1-km resolution land use/land cover (LULC) map from the Data Center for Resources and Environmental Sciences, Chinese Academy of Sciences, is used to determine fractions of four main land cover types (grass, farmland, bare soil, and forest). Land cover sensitivity snow depth retrieval algorithms are initially developed using AMSR-E brightness temperature data. Each grid-cell snow depth was estimated as the sum of snow depths from each land cover algorithm weighted by percentages of land cover types within each grid cell. Through evaluation of this algorithm using station measurements from 2006, the root mean square error (RMSE) of snow depth retrieval is about 5.6 cm. In forest regions, snow depth is underestimated relative to ground observation, because stem volume and canopy closure are ignored in current algorithms. In addition, comparison between snow cover derived from AMSR-E and FY3B-MWRI with Moderate-resolution Imaging Spectroradiometer (MODIS) snow cover products (MYD10C1) in January 2010 showed that algorithm accuracy in snow cover monitoring can reach 84%. Finally, we compared snow water equivalence (SWE) derived using FY3B-MWRI with AMSR-E SWE products in the Northern Hemisphere. The results show that AMSR-E overestimated SWE in China, which agrees with other validations.

snow depth, passive microwave, FY3B-MWRI, China

Citation: Jiang L M, Wang P, Zhang L X, et al. 2014. Improvement of snow depth retrieval for FY3B-MWRI in China. Science China: Earth Sciences, 57: 1278−1292, doi: 10.1007/s11430-013-4798-8

Snow cover is a key parameter with significant impact on climate, weather and water resources. Given its high albedo and melting characteristics, it can greatly alter the surface radiation balance, which has pronounced effects on heat and moisture fluxes between land surface and atmosphere. Microwaves can penetrate clouds in the atmosphere and this gives the opportunity to derive snow water equivalence (SWE) or snow depth information under all weather conditions (Foster et al., 1984). Satellite-borne passive microwave sensors have been used to produce snow cover information since 1978, including the Scanning Multichannel Microwave Radiometer (SMMR) aboard Nimbus-7, the Special Sensor Microwave Imager (SSM/I) on a series of Defense Meteorological Satellite Program satellites, the Tropical Rainfall Measuring Mission Microwave Imager, and the Advanced Microwave Scanning Radiometer-EOS (AMSR-E). The Fengyun-3B (FY3B) meteorological satellite was launched on 5 November 2010. Combination of the previous four sensors and the Microwave Radiation Imager (MWRI) aboard FY3B is expected to provide time series of snow cover on land. This represents a new data source for the research fields of climate and hydrology. AMSR-E observation was halted on 4 October 2011. AMSR2 is the

*Corresponding author (email: jiang@bnu.edu.cn)

successor to AMSR-E, aboard the Global Change Observation Mission 1st—Water "SHIZUKU" (GCOM-W1). It was launched on 18 May 2012. AMSR2 data will be released after completion of a calibration and validation phase, which will require about one year. FY3B-MWRI is one of the major sensors providing surface brightness temperature. Associated work developed a semi-empirical snow depth retrieval algorithm over China, using the physical relationship between brightness temperature difference and snow depth. This technique takes into account different land type compositions in the passive microwave footprint.

Snow cover or snow depth estimation using passive microwave sensors has been investigated over the past three decades. At lower frequencies of the microwave band, emission from dry snow cover is mainly affected by underlying soil dielectric and roughness properties; however, at higher frequencies, emission is sensitive to SWE and snow particle size, since volume scattering by snow particles becomes important (Hofer et al., 1980; Rott et al., 1991). Current SWE algorithms using passive microwave data often use linear semi-empirical regression between brightness temperature difference and snow depth (Chang et al., 1976, 1987; Hallikainen et al., 1992). The most used frequencies are 36 GHz (or 37 GHz) and 18 GHz (or 19 GHz). Foster et al. (1997) improved SWE mapping in forest areas by incorporating forest fraction. Tait (1998) estimated SWE in 16 land cover categories, using SSM/I brightness temperature and *in situ* snow depth data from sites in the United States and Russia. Influences included snow wetness, depth hoar, complex mountainous terrain, and dense forest cover. Sixteen separate semi-empirical SWE models for each category were established, using the brightness temperature difference between 19, 36 and 85 GHz. Their results showed that SWE errors for surface cover without melting or depth hoar that are non-forested and noncomplex are smallest among all ground types, with correlation coefficient 0.75. SWE estimated over land surfaces covered by wet snow, depth hoar and non-forested and complex mountainous terrain had large errors, with correlation coefficient 0.22. This demonstrated the effect of land surface types on SWE retrieval. Singh et al. (2000) improved a SWE algorithm for the Red River Basin of North Dakota and Minnesota by incorporating elevation and atmospheric temperature and precipitable water, and by removing areas affected by large water bodies and depth hoar. Derksen et al. (2005) developed land cover sensitivity SWE retrieval algorithms, applying them to both SMMR and SSM/I data in Canada. At each grid cell, SWE estimates were the sum of values from four individual land cover algorithms (deciduous forest, coniferous forest, spare forest, and open prairie), weighted by the percentage of each type. For the tundra area, Derksen et al. (2010) developed an algorithm dependent only on V-polarization brightness temperature in the 37 GHz channel, using winter observations from March 2002– July 2006.

SWE retrieval algorithms for China have been studied during the past two decades. Cao et al. (1993) adjusted the coefficients of Chang's algorithm (Chang et al., 1987) for western China, using SSMR brightness temperature. Using digital elevation model (DEM) data, they classified five areas: high mountains, plateau, low mountains, rolling hills and basin. Che et al. (2008) modified Chang's algorithm using 1980–1981 ground observations for SSMR, and 2003 for SSM/I. They considered influences of vegetation, wet snow, precipitation, cold desert and frozen ground on snow depth estimation. Root mean square errors (RMSE) of their estimates were 6.22 and 5.22 cm for SSMR and SSM/I, respectively.

It has been demonstrated that snow cover is important in modifying regional and possibly remote climate by changing the surface energy balance, because the calculated surface albedo of snow surfaces depends on the snow cover fraction. There are empirical relationships between snow depth and snow fraction in general circulation model (GCM) grid cells or sub-grid cells (Liston, 2004; Wu et al., 2004). Wu et al. (2004) quantified snow cover fraction parameterization in a GCM using snow depth generated via SSMR 37 GHz and 18 GHz channels. Sun (2007) and Chang et al. (2009) developed an empirical snow depth algorithm using AMSR-E, by incorporating MODIS 8-day snow-covered fraction data (MYD10A2). In the work of Sun (2007), China was divided into three snow regions. The semi-empirical snow depth retrieval algorithms for these regions were developed individually. In the Xinjiang region, snow fraction was integrated into the regression of snow depth retrieval. Through validation, estimated error decreased when snow fraction was included. Using the work of Sun (2007), Chang et al. (2009) improved snow depth retrieval techniques for four different land types, using MODIS land cover product MOD12Q1 V004. The brightness temperature difference between 18.7 and 89 GHz is also included in snow depth algorithms to detect shallow snow. This algorithm is valid with a snow layer thicker than 3 cm. Its RMSE is small, 5.6 cm. However, this algorithm is unsuitable for monitoring snow cover in real time, since it requires 8-day MODIS snow cover data (MYD10A2).

To estimate real-time snow depth, we propose a semi-empirical algorithm using only passive microwave remote sensing observations. We use a land use/land cover (LULC) map from 2000 (with grid cell size 1 km×1 km) from the Data Center for Resources and Environmental Sciences (RESDC), Chinese Academy of Sciences. Based on 7-year (2002–2009) observations of brightness temperature (AMSR-E) and snow depth (from meteorological stations) in China, we developed a semi-empirical snow depth algorithm for FY3B-MWRI.

1 FY3B-MWRI

The FY3B satellite with microwave radiation imager

(MWRI) has the purpose of detecting rain rate, cloud water content, total water vapor, soil moisture, sea ice concentration, sea surface temperature, and snow depth. Tables 1 and 2 list operational parameters of the AMSR-E and FY3B-MWRI sensors, respectively. The sensors have similar performance settings, except that FY3B-MWRI is missing the 6.925 GHz channel, and its spatial resolution and sensitivity are lower than that of AMSR-E. However, FY3B-MWRI data are easily accessible to domestic users, making it possible to produce higher temporal resolution estimates in the China area. This work will not only help accelerate improvement and development of the domestic passive microwave sensor instrument, but also promote applications in snow disaster monitoring.

We develop a semi-empirical snow depth retrieval algorithm based on characteristics of the FY3B-MWRI sensor. However, because FY3B-MWRI has provided passive microwave brightness temperature data only since December 2010, it is not possible to develop a reliable statistical regression based on the limited data from the FY3B-MWRI project thus far. AMSR-E and FY3B-MWRI cross the equator in a descending mode at about 1:30 p.m. local time. Hence, AMSR-E data can substitute for FY3B-MWRI to establish a statistical snow depth regression algorithm for the latter instrument. From Tables 1 and 2, it is seen that the sensitivity, noise and footprint size of the MWRI sensor are not as good as those of AMSR-E. However, Yang et al. (2011a, 2011b) used a double-difference method to evaluate MWRI with WINDSAT. Biases were generally less than 2 K. From comparison of FY3B-MWRI with AMSR-E, mean bias between the two sensors is about 0.13–2.13 K, with maximum bias −2.19 K in the 37-H and 89-H channels (Yang et al., 2011b). FY3B-MWRI observation accuracy is affected by many factors, such as receiver gain drift, standard calibration source brightness temperature accuracy, calibration accuracy, and efficiency of the main antenna beam. Therefore, Sun (2007) accounted for sensitivity of the current SWE algorithm to the sensor configuration of FY3B-MWRI by adding ±6 K Gaussian noise to the brightness temperature. Through testing AMSR-E official SWE products, RMSE was found less than 4.6 mm. There was more sensitivity to negative noise than positive. Expected SWE accuracy of AMSR-E is reported at 20% (or 10 mm). Therefore, FY3B-MWRI observation bias with respect to AMSR-E should not affect snow depth retrieval accuracy. Thus, the snow depth estimation technique established by combining AMSR-E data with ground snow depth measurements can be directly applied to FY3B-MWRI.

2 Theory

The passive microwave brightness temperature of snow-covered terrain is influenced by numerous factors other than amount and structure of snow, which include soil properties, vegetative cover and atmospheric conditions (Foster et al., 1984). Scattering of dry snow cover dominates at high microwave frequencies. At low frequencies (snow-particle size much smaller than wavelength), absorption is the primary loss, whereas at high frequencies (snow-particle size of the same order of magnitude as wavelength), scattering dominates. Based on the radiative transfer model and Mie scattering theory, scattering is extremely sensitive to changes in grain-size; for a snow particle of diameter 1 mm, scattering dominates at frequencies above 15 GHz (Ulaby et al., 1981). Given the sensitivity of snow depth and water volume at

Table 1 The operating characteristics of AMSR-E

Frequencies (GHz)	6.925	10.65	18.7	23.8	36.5	89
Footprint size (km)	75×43	51×29	27×16	32×18	14×8	6×4
Beamwidth (MHz)	350	100	200	400	1 000	3 000
Polarization	V/H	V/H	V/H	V/H	V/H	V/H
Sensitivity (K)	0.34	0.7	0.7	0.6	0.7	1.2
Accuracy (K)	1	1	1	1	1	1
Incidence angle (°)				55		
Swath width (km)				1445		

Table 2 The operating characteristics of FY3B-MWRI

Frequencies (GHz)	10.65	18.7	23.8	36.5	89
Footprint size (km)	51×85	30×50	27×45	18×30	9×15
Beamwidth (MHz)	180	200	400	900	2300
Polarization	V/H	V/H	V/H	V/H	V/H
Sensitivity (K)	0.6	1	1	1	2
Accuracy (K)	1.2	2	2	2	2.8
Incidence angle (°)			53		
Swath width (km)			1400		

different frequencies, the brightness temperature difference of 18.7 and 36.5 GHz is used to estimate SWE. Since there is extensive coverage of shallow snow depths in China, we used the 89 GHz channel to detect such shallow snow. Shuman et al. (1993) found that the polarization ratio at 37 GHz (T_{B37V}/T_{B37H}) changed distinctly during periods of surface hoar and depth hoar formation. Koenig et al. (2004) improved SWE estimation in Alaska, USA using SSM/I by incorporating the polarization difference of 37 and 85 GHz, because of its strong sensitivity to depth hoar. This is because the scattering character of depth hoar is similar to that of surface hoar, and the existence of hoar increases reflectivity at H-polarization but has no impact on V-polarization. Therefore, when the snow surface is covered with depth hoar, use of the polarization difference between 37 and 89 GHz improves SWE estimation. If average monthly air temperature is less than −10°C and snow depth less than 0.1–0.5 m, depth hoar forms between the snow and ground surface (Koenig et al., 2004). Average monthly temperature of the Qinghai-Tibet Plateau and Xinjiang from December through February is usually colder than −10°C, and there is deep depth hoar across most of these areas. In addition, the brightness temperature difference between 18.7 and 10.7 GHz has strong sensitivity to deep snow (Derksen, 2008; Kelly, 2009). Therefore, four frequencies are used to establish the snow depth statistical regression algorithm for China.

Given the coarse footprint (tens of km) of a satellite microwave radiometer, measured brightness temperature usually represents several land cover types. This mixed-pixel problem is the dominant limitation on snow depth and SWE estimation accuracy using passive microwave measurements. These measurements have a similar problem caused by spatial heterogeneity. The physical process of emission, given by the Planck equation, requires a large microwave radiometer pixel with sufficiently high number of photons to measure. Different land cover types will affect the aggregation and distribution of snow. There are studies that have obtained snow depth over different forest types (Derksen et al., 2005; Goita et al., 2003). Derksen et al. (2005) acquired snow depth at a satellite pixel, through summarizing sub-grid cell snow depth for each land cover type. Our snow depth algorithm for China is developed using a mixed-pixel decomposition technique.

According to the LULC map, the land surface is divided into four types: grassland, farmland, bare ground, and forest. At each grid cell, snow depth is estimated from the sum of snow depth values from each land cover algorithm, weighted by the percentage of land cover type within each grid cell:

$$\mathrm{SD}=f_{\mathrm{grass}}\times\mathrm{SD}_{\mathrm{grass}}+f_{\mathrm{barren}}\times\mathrm{SD}_{\mathrm{baren}}+f_{\mathrm{forest}}\times\mathrm{SD}_{\mathrm{forest}}+f_{\mathrm{farmland}}\times\mathrm{SD}_{\mathrm{farmland}}, \quad (1)$$

where f_{grass}, f_{barren}, f_{forest}, and f_{farmland} are area fractions of grassland, bare ground, forest, and farmland in each grid cell, respectively. $\mathrm{SD}_{\mathrm{grass}}$, $\mathrm{SD}_{\mathrm{barren}}$, $\mathrm{SD}_{\mathrm{forest}}$, and $\mathrm{SD}_{\mathrm{farmland}}$ are snow depths for each type, from the snow depth retrieval algorithm at the pure pixel. We assume that a pixel is pure when a certain cover type comprises more than 85% of its total area.

3 Data and processing

The data used include the year 2000 1-km LULC map, *in-situ* snow depth and surface temperature measurements, plus AMSR-E brightness temperature. All these data were reprojected into a Lambert azimuthal equal-area projection (Table 3). The spatial coverage is 15.5°–51.5°N and 64.5–123.5°E. Grid cell size is 23.1656 km × 23.1656 km.

3.1 LULC map

The LULC data is freely available from the RESDC. The data are in ESRI ArcInfo GRID format, with ground pixel size 1 km×1 km, and derived from 30 m Thematic Mapper (TM) imagery classification. The LULC classification system corresponds to national first-level and second-level classification standards. There are 25 land cover types in all, including farmland, woodland, grassland, water body, and residential area. Area percentages of each land cover type in China are presented in Table 4, which shows that the major types are grassland, farmland, bare ground, and forest. Hence, the snow depth statistical inversion algorithm for these four main land cover types is established first.

Figure 1 shows maps of grassland, forest, farmland and bare ground. Because these maps were derived from 30-m

Table 3 The map projection for snow depth product used in China

Parameters	Value
Projection	Lambert azimuthal equal area
False easting	0
False northing	0
Central meridian (°)	100
Latitude of origin (°)	45
Linear unit	meter
Datum	WGS-1984

Table 4 Percentage of each land cover type in 2000 LULC map

Land type	Percentage (%)
Grassland	31.7
Farmland	18.94
Bare rock and Gobi desert	11.48
Sandy land	6.33
Forest	18.06
Shrub	5.55
Saline soil	1.44
Cities	1.81
Wetlands	0.86
Others	0.97
Water bodies	1.55
Permanent ice and snow	0.73
Beaches	0.53
Shoals	0.06

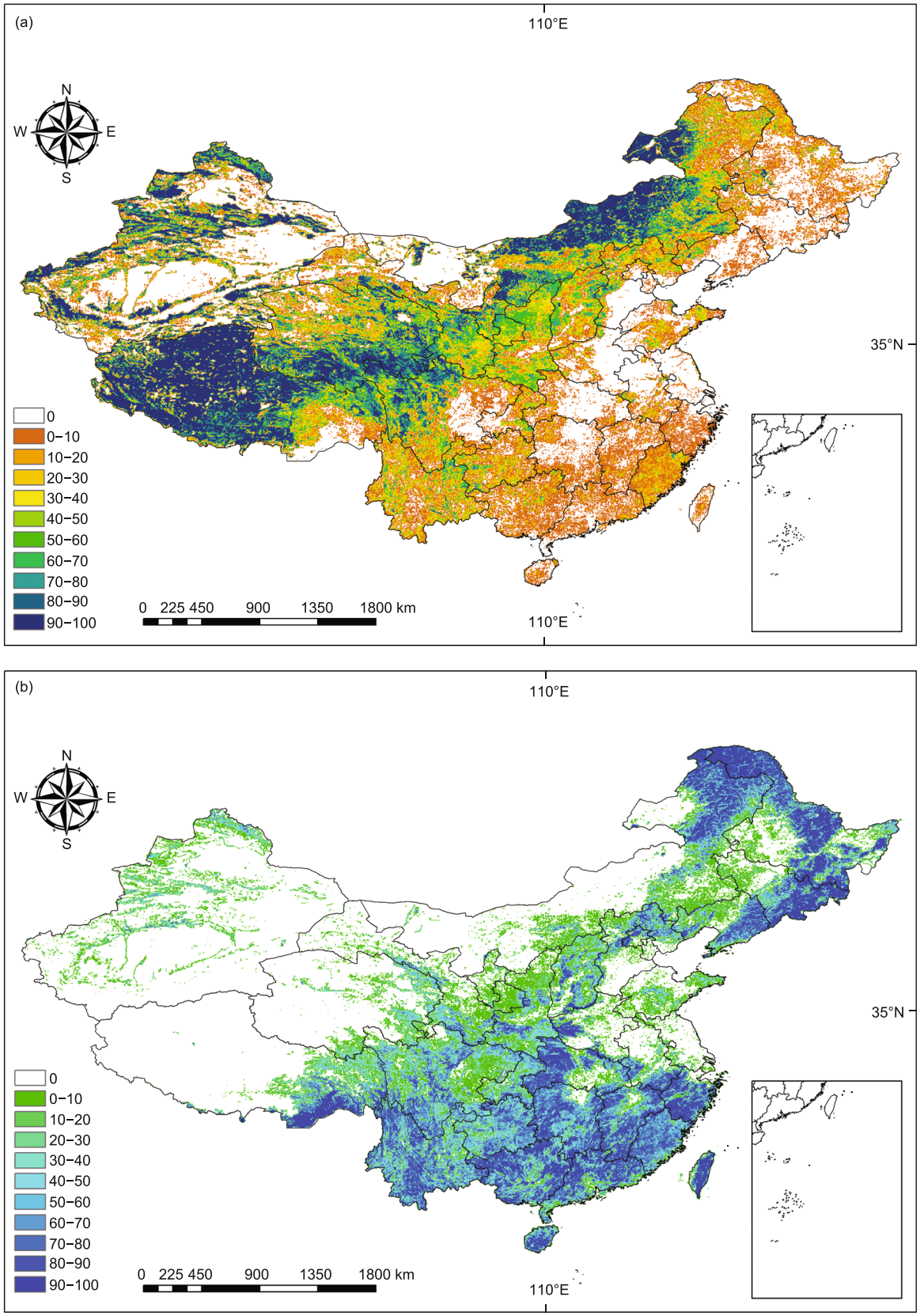

Figure 1 (a) Grassland map in 2000; (b) forest map in 2000; (c) farmland map in 2000; (d) map of bare ground in 2000.

(*To be continued on the next page*)

(*Continued*)

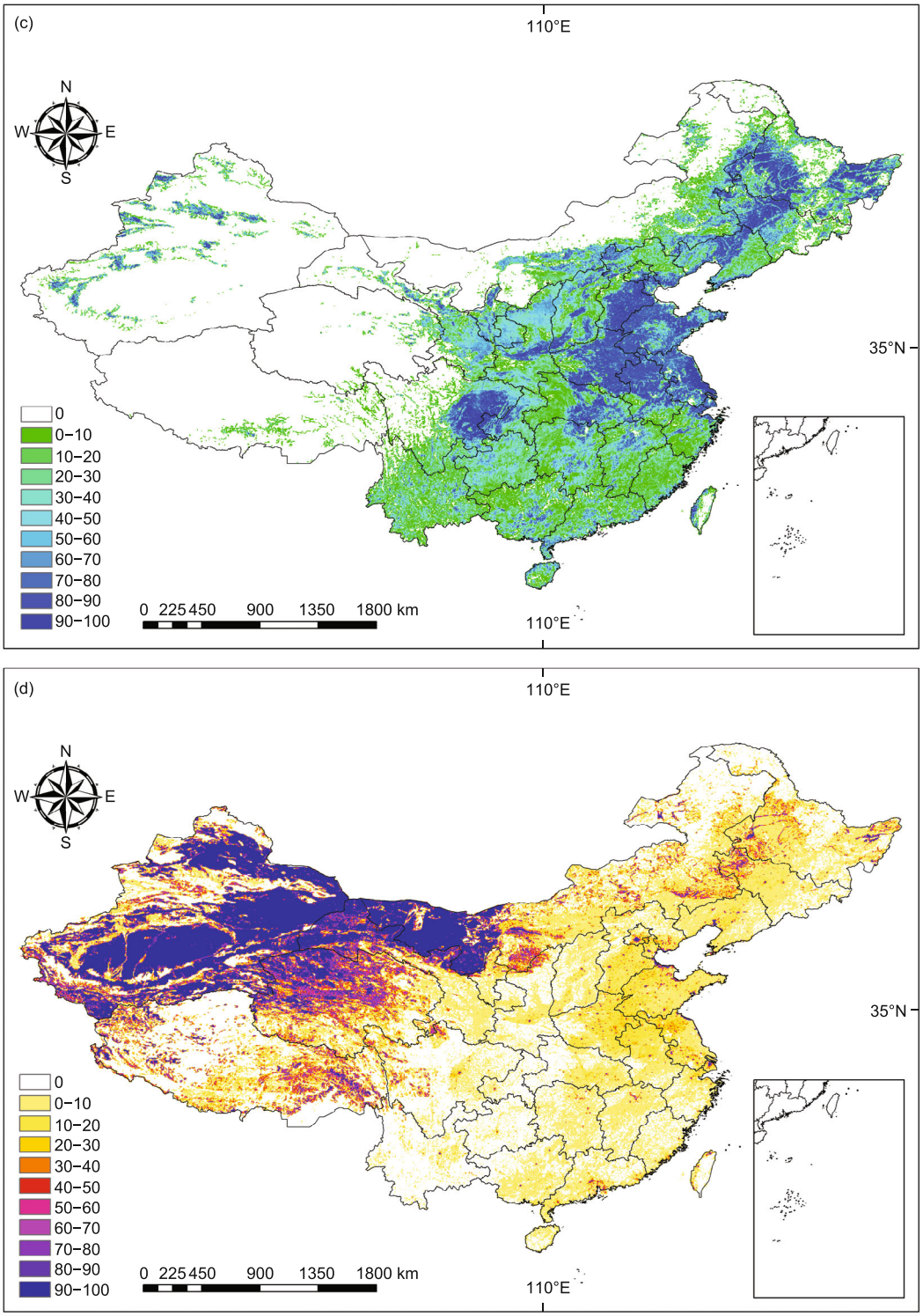

TM imagery, they can be recalculated as percentages of each land cover type in 25 km grid cells. Furthermore, the China vegetation atlas confirms that the RESDC LULC map describes the surface in the region more accurately than its MODIS counterpart.

From the grassland percentage map (Figure 1(a)), the LULC data show that grasslands of the Qinghai-Tibet and Yunnan-Guizhou plateaus are substantially more consistent with vegetation maps. From the forest percentage map (Figure 1(b)), Northeast China has the important natural forest areas, especially in the Daxinganling, Xiaoxinganling, and Chang-baishan mountains. The LULC data provide a good

overview of the distribution of these forests. From the farmland map (Figure 1(c)), farmland is mainly across Northeast and Southeast China. Bare ground coverage is concentrated in the northwest (Figure 1(d)), consistent with the actual surface distribution.

Although the LULC map is about ten years older than data input to our SWE retrieval models, it appears to work well for our purposes, because that map has changed little over the past decade. Since we did not acquire the latest Chinese LULC maps, we used the MODIS International Geosphere Biosphere Programme (IGBP) products to investigate changes over the period 2001–2010, in particular MODIS land cover type product MCD12Q1. MCD represents land cover produced from combination of two MODIS sensors on both Aqua and Terra. Its spatial resolution is 500 m (Collection 5 product). Figure 2 shows MODIS land cover maps in 2001 and 2010. It is seen that there was 15.12% forest, 39.58% grassland, 19.59% farmland, and 25.71%

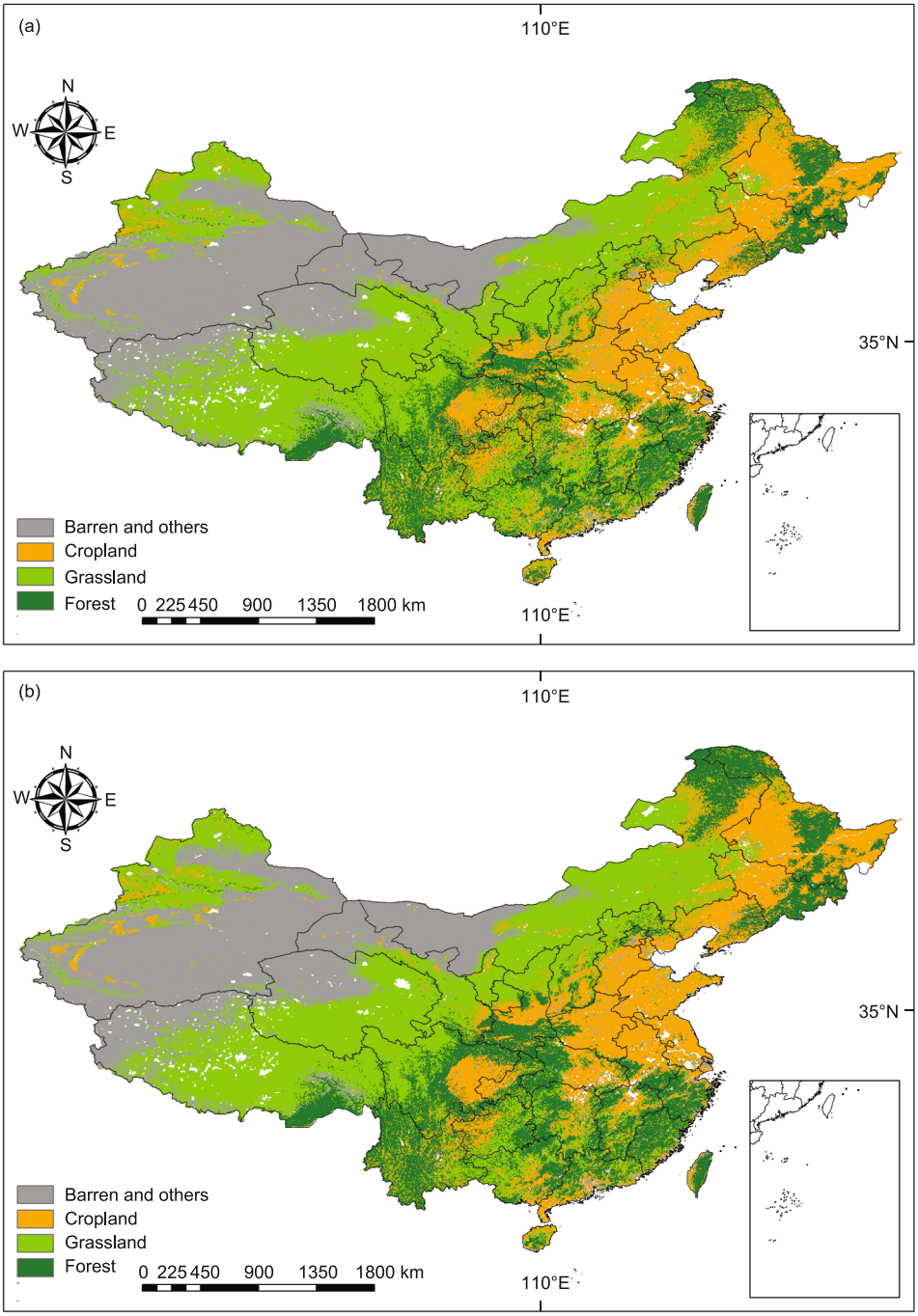

Figure 2 Land cover maps of MODIS IGBP products. (a) 2001; (b) 2010.

bare ground in 2001. In 2010, corresponding areal percentages were 17.99%, 37.01%, 20.12%, and 24.88%. Between 2001 and 2010, maximum change was about 2% for forest and grassland regions. Areas of farmland and bare ground changed even less, both smaller than 1%. The most obvious changes of LULC over the period were mainly in Northeast and Central China. Forest percentages in both regions increased over the period, while farmland varied little. We conclude that such land cover change over nearly 10 years is negligible for our SWE retrieval. Therefore, it is reasonable to use the 2000 RESDC LULC map version as land classification input data to develop our snow depth retrieval algorithm.

3.2 Weather station observations

Weather station data were acquired from the National Meteorological Information Center, China Meteorology Administration (CMA). Data from 753 stations (Figure 3) were used. The observation period is from 2002-06-01 to 2009-12-11. Recorded variables include site name, observation time, site location (latitude and longitude in degrees), geodetic elevation (m), surface temperature, snow depth (cm), and snow pressure (g cm^{-2}). A month field of "999" means a missing snow depth observation for that month; an "888" indicates no snow, and a "988" denotes little snow.

Sites were selected from three seasonal snow cover regions, mainly in Xinjiang, Northeast China and Inner Mongolia, and the Tibetan Plateau. There are few snowfalls in southern China, which are usually in the form of wet snow. Here, there are also vast and widely distributed water bodies. Hence, only a few stations in southern China were chosen for snow depth retrieval algorithm development. To ensure snow depth data for solely dry snow, only measurements from late October through March were used.

Observation data quality control was done using several criteria. Records with missing information were deleted, and records were selected only if surface temperature was less than 0°C (to avoid the impact of wet snow) and snow pressure greater than 0 g cm^{-2}. Then, the site data were reprojected into the Lambert equal-area projection, to match the AMSR-E L2A (Level-2A) brightness temperature data and LULC map.

3.3 Passive microwave brightness temperature data

The AMSR-E L2A brightness temperature dataset was downloaded from the National Snow and Ice Data Center (NSIDC). It contains brightness temperatures at 6.9, 10.7, 18.7, 23.8, 36.5, and 89.9 GHz frequency channels. Data grids were resampled to be spatially consistent, and are available at various spatial resolutions corresponding to footprint size of the observations, such as 56, 38, 24, 21, 12, and 5.4 km. Data are stored in Hierarchical Data Format-Earth Observing System (HDF-EOS) format.

To correspond with the ground data period, the brightness temperature data are from 2002-06-01 to 2009-12-11. Spatial resolution of AMSR-E L2A brightness temperature for each frequency is Resolution 2 (about 37 km). Data from 2006 were used for algorithm validation, and data from other years used for algorithm development.

Geographic location information of stations was used to search corresponding brightness temperature pixels in AMSR-E imagery. Here, we used the nearest neighbor searching algorithm to find the pixel over the ground station location. AMSR-E L2A brightness temperature data points were binned into one Lambert equal-area grid via the nearest neighbor method.

There are three and half granules of AMSR-E brightness temperature data covering China each day. Hence, there are missing data in daily snow depth mapping of the country. Therefore, not all daily snow depth ground observations are

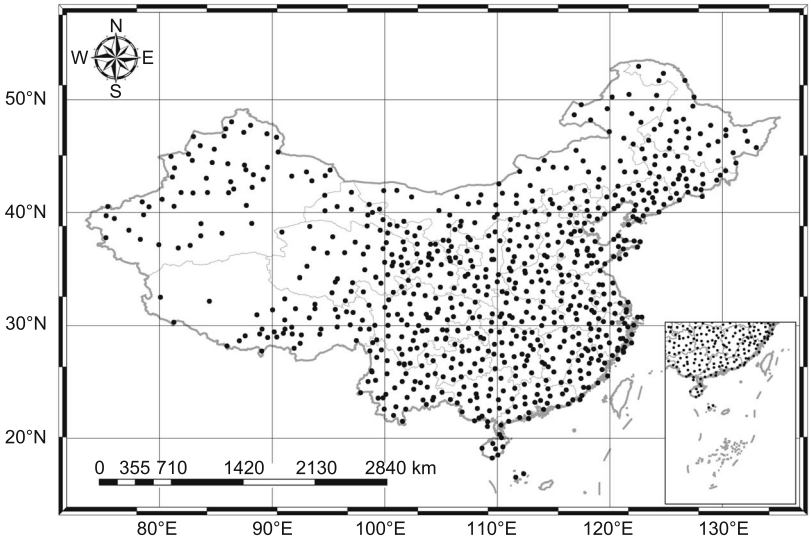

Figure 3 China meteorological stations used in this work.

matched with corresponding microwave brightness temperature data.

4 Algorithm development

Snow has a scattering behavior similar to frozen soil, cold desert and rainfall (Grody, 1991; Grody et al., 1996). Thus, the impact of these should be excluded before estimating snow depth. The snow depth inversion technique is based on emission characteristics of dry snow at different frequencies. Consequently, accuracy of the linear regression algorithm depends on determination of dry and wet snow conditions.

Grody et al. (1996) developed a global snow identification method using SSM/I measurements. This method was used in deriving the AMSR-E official SWE product (Kelly, 2009). Li et al. (2007) improved Grody's method (Grody et al., 1996) with SSM/I data and ground station observations in China. With approximately 6-year snow measurements from these stations and operational snow cover products for Inner Mongolia from the National Satellite Meteorological Center (NSMC) of China, they developed a modified method for the China region. A new index, $(T_{B22v}-T_{B85v})-(T_{B19v}-T_{B37v})$, was added. This effectively reduced the influence of frozen ground on snow depth estimation on the Qinghai-Xizang Plateau. Hence, we applied Li's snow cover identification method (Li et al., 2007) to remove scattering signals from frozen ground, cold desert and rainfall in the development of our snow depth retrieval. Brightness temperature data were used to establish the regression snow depth algorithm only when a grid cell was determined to have dry snow cover.

With water bodies within a snow-covered grid cell, satellite-observed brightness temperature decreases significantly because of the low emissivity of water. This reduces the difference of brightness temperature between 18.7 and 36.5 GHz. This is opposite the $T_{B19}-T_{B37}$ of dry snow cover. Therefore, a large water body in a grid cell produces large error in snow depth retrieval. The land-ocean-coastlines-ice (LOCI) mask was therefore used to remove data of pixels containing water bodies.

There are few relatively pure pixels at pixel size 25 km, so it is difficult to establish a regression algorithm for a single land cover type Therefore, if a land cover percentage was greater than 85% within one grid cell, we assumed this cell to be a pure pixel of that cover type.

Moreover, there is no snowmelt status (wet/dry) information in ground observations. Wet snow usually occurs in early winter or late spring melt periods. Records of either daily maximum air temperature or maximum surface temperature greater than 0°C in ground-based observation records were excluded, to remove the effect of wet snow on the snow retrieval algorithm. During the snow depth inversion, wet snow is included but flagged as such.

All frequencies, 10.7, 18.7, 36.5 and 89 GHz at both polarizations, were used for the regressions of empirically derived algorithms. The 10.7 and 18.7 GHz channels are sensitive to underground surfaces, and 36.5 GHz is sensitive to snow volume scattering. The 89 GHz channel was added because of its penetrability of shallow snow. After removing wet snow and other scattering, there were about 60% of records with snow depths less than 10 cm remaining from the original data. These data were used for snow depth inversion algorithm development.

The snow depth regression algorithm was formulated using 7 years of observations (2002–2005 and 2007–2009). Observations from 2006 were used to validate the new algorithm.

Through statistical regression analysis of various underlying "pure" land cover surfaces, we determined a snow depth inversion algorithm for the four land types. These regressions are as follows.

$$SD_{farmland}=-4.235+0.432\times d18h36h+1.074\times d89v89h; \quad (2(a))$$

$$SD_{grass}=4.320+0.506\times d18h36h-0.131\times d18v18h+0.183\times d10v89h-0.123\times d18v89h; \quad (2(b))$$

$$SD_{bare\ soil}=3.143+0.532\times d36h89h-1.424\times d10v89v+1.345\times d18v89v-0.238 d36v89v; \quad (2(c))$$

$$SD_{forest}=11.128-0.474\times d18h36v-1.441\times d18v18h+0.678\times d10v89h-0.649\times d36v89h; \quad (2(d))$$

where $SD_{farmland}$, SD_{grass}, $SD_{bare\ soil}$, and SD_{forest} are estimated snow depths for farmland, grass, bare ground and forest surfaces, respectively. The unit of depth is centimeters (cm), and d is the brightness temperature difference of two frequencies. The numbers 10, 18, 36, and 89 represent the AMSR-E frequencies; v is V-polarization, and h is H-polarization. For example, d18v36h means the brightness temperature difference between 18.7 GHz V-pol and 36.5 GHz H-pol, i.e., $Tb_{18v}-Tb_{36h}$.

Farmland and grass are short vegetation, and their contributions to observed emission from snow surfaces are small. Therefore, snow depth in farmland and grassland is highly correlated with the brightness temperature difference between the 18.7 and 36.5 GHz channels. Bare ground typically has only shallow snow cover, with the majority of snow depths less than 10 cm. Hence, the use of high frequency bands (36.5 and 89 GHz) can greatly improve depth retrieval for bare soil surfaces. Moreover, the brightness temperature difference between 36.5 and 89 GHz ($Tb_{36.5}-Tb_{89}$) is used in eq. (2), because the polarization difference at high frequency detects surface hoar and depth hoar (Koenig et al., 2004). For forested area, the brightness temperature of cross-polarization is more sensitive to snow depth than that of co-polarization, owing to the dual effects of complex terrain and forest cover. RMSE of the snow depth inversion algorithm for four land types is listed in Table 5. Although all regressions pass the 95% confidence

Table 5 Statistic evaluation of four main snow depth algorithms over four land cover types

Land cover	Regression (R^2)	Regression RMSE (cm)	Regression samples	Validation samples	Validation RMSE (cm)
Farmland	0.44	4.36	2888	448	4.51
Grassland	0.58	3.57	2894	505	2.74
Bare ground	0.59	2.15	177	40	1.82
Forest	0.16	5.60	1163	188	6.11

level test, the algorithm shows poor performance in forest areas. A possible reason may be the relatively poor representation of selected meteorological stations in forested regions at satellite scales. Further, because emission of the forest area increases with frequency, the brightness temperature difference shows few variations there. Therefore, the snow depth inversion algorithm performs worse for forested surfaces than for the other three land types.

5 Validation of snow depth algorithms

5.1 Validation of snow depth algorithms for "Pure" land types

Since there was no extreme blizzard or snowstorm in 2006, observations from this year were used to evaluate the developed algorithms. After identifiying snow cover using Li's method (Li et al., 2007), site observations of pure pixels were used to validate the algorithms for each land cover type. Comparisons between estimated snow depth and ground station observations for grassland, farmland, bare ground, and forest cover types are shown in Figure 4, respectively, from which it is seen that the snow depth inversion algorithms perform better for grassland and farmland, since both surfaces are relatively flat and have smaller vegetation impacts on the inversion regression. The RMSE of snow depth retrieval for grass surfaces is only 2.74 cm, and 1.82 cm for bare surfaces. Snow depth retrieved for forested areas is underestimated compared to ground observations. This is because forest cover produces a smaller brightness temperature difference between frequencies, which limits the algorithm using this difference. Another explanation for large retrieval errors over forested areas is that both complex terrain and trees have negative impacts on retrieval there. Indeed, forests are commonly found in mountainous regions, such as the Daxiaoxing' anling and Taihang mountains. Moreover, the emission of forest depends on stem volume, canopy closure, and others.

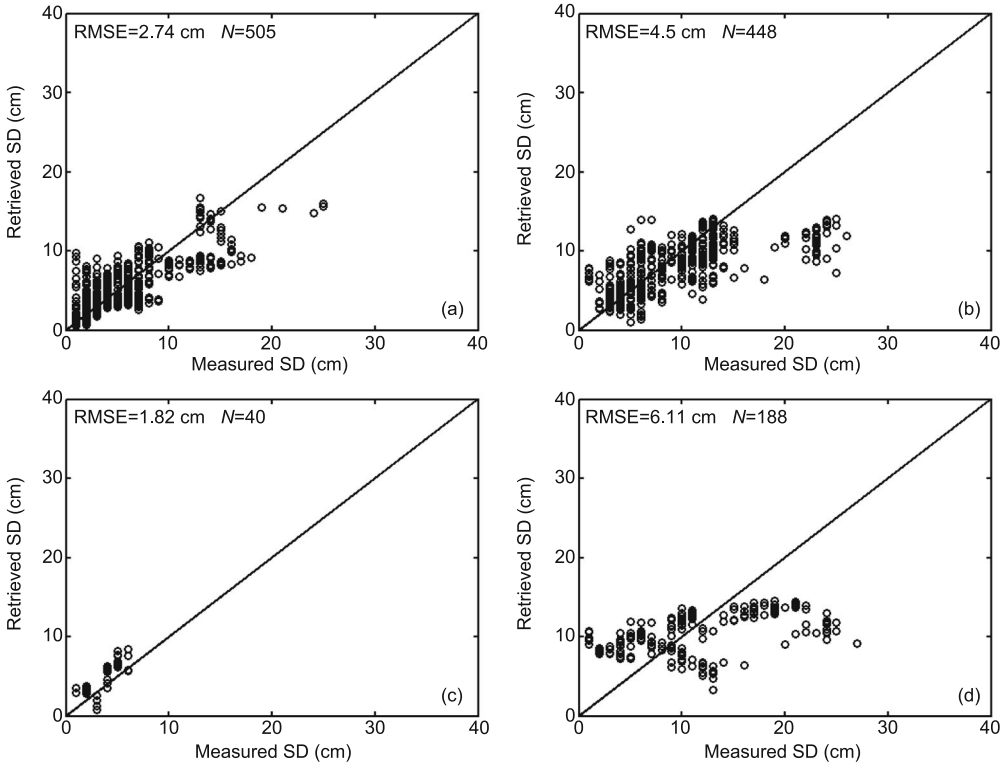

Figure 4 (a) Comparison of estimated and observed snow depths in different land surfaces. (a) Grassland; (b) bare ground area; (c) farmland; (d) forest.

The physical relationship between them is still unclear in current emission models, so more study is needed before such factors can be incorporated in the retrieval algorithms.

Table 5 gives the RMSE of snow depth for the four land types. There were few samples of bare ground for algorithm regression and validation (only forty for the validation). RMSE is about 2 cm over this ground, and estimated snow depth agrees well with station measurements.

5.2 Algorithm validation for mixed pixels

To evaluate the overall behavior of the snow depth algorithm in the satellite applications, observational data from 521 sites in 2006 as mixed pixels were used for algorithm evaluation. The number of snow samples for validation was 3438. A comparison of estimated snow depth with observations is shown in Figure 5. The RMSE is about 5.6 cm for mixed pixels. For shallow snow surfaces, the inversed snow depths are scattered. This is because of the complex nature of these surfaces and the highly variable composition patterns within a satellite grid. Second, ground stations are usually located close to cities and on flat terrain. Thus, station observations may not be representative of the average snow conditions of the overlying pixel, with its associated errors. Third, grid resolution of passive microwave sensors is relatively coarse. Sample points in each swath are reprojected into a grid of cell size 25 km×25 km, using a weighted averaging method. Areas adjacent to the location of brightness temperature data will be projected into the same grid. Passive microwave pixel resampling error is large. The impact of these three factors is not considered in current techniques, so further study is required. In addition to the evaluation of inversion algorithms with snow depth observations using RMSE, we produced a histogram of inversion error. Figure 6 shows a histogram of retrieved snow depth bias, which follows a statistically normal distribution. It is seen that bias is within ±5 cm.

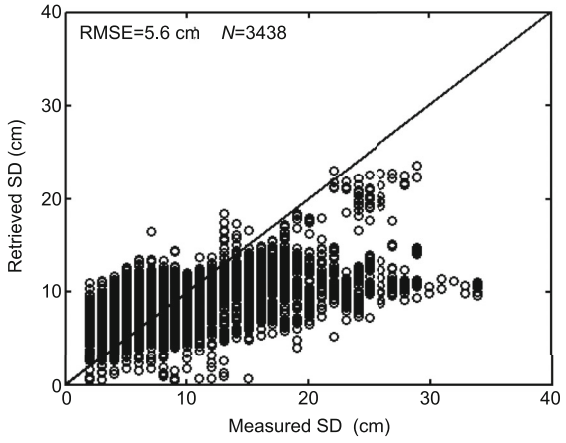

Figure 5 Validation of snow depth retrieval with ground observations over mixed-pixels.

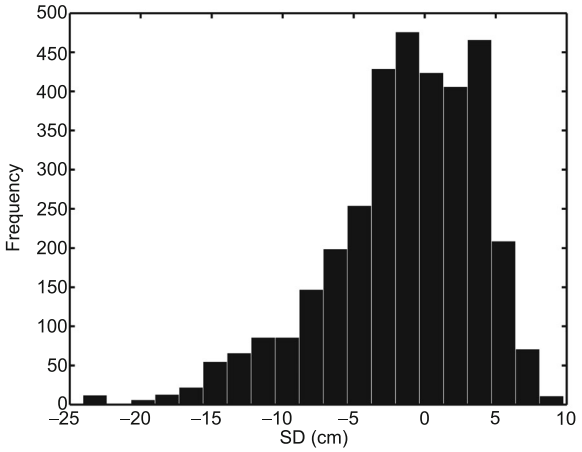

Figure 6 Histogram of root mean square error of snow depth over mixed-pixels.

5.3 Evaluation of snow cover retrieval using the developed algorithm

The snow depth algorithm was validated with site observations, and further evaluated with MODIS daily snow cover products for snow cover spatial distribution consistency. MODIS daily global climate-modeling gridded snow products (MYD10C1) have 0.05° resolution. We selected the data period to be consistent with AMSR-E and FY3B-MWRI, from 2010-11-01 to 2011-02-28. For this comparison, the snow depth algorithms developed here used both AMSR-E and FY3B-MWRI data. A pixel with snow depth greater than zero, estimated from the passive microwave sensors, was considered snow-covered. MYD10C1 snow cover products were converted to the Lambert equal-area projection.

The MODIS daily snow cover product is often contaminated by clouds. There were 92.82% of snow pixels so affected, and 24.49% had 80% cloud coverage. During the accuracy evaluation using microwave and optical snow cover products, it was necessary to account for cloud impacts. The comparisons are detailed as follows. First, we ensured that MYD10C1, AMSR-E and FY3B-MWRI all covered the same period; second, both optical and microwave snow cover data were resampled to the Lambert projection. AMSR-E and FY3B-MWRI data that were missing or over water bodies were removed. There were 74 matching days between MODIS snow cover and AMSR-E products but only 35 matching days between MODIS and FY3B-MWRI, since the swath of the latter is narrower than that of the former. Third, MODIS snow pixels were determined as follows, given the cloud contamination. For snow coverage greater than 85% within a pixel, that pixel was considered snow-covered; for zero snow coverage and cloud amount not in excess of 15%, the pixel was classified as snow-free.

Through comparison of MODIS snow products with AMSR-E and FY3B-MWRI, overall accuracy of the

AMSR-E product was 88.54% and that of FY3B-MWRI 84.66 %.

Snow-covered and snow-free classification accuracy of AMSR-E was calculated as

$$\frac{6006+339023}{389680}\times 100\% = 88.54\%.$$

Snow-covered and snow-free classification accuracy of FY3B-MWRI was calculated as

$$\frac{4110+106796}{130998}\times 100\% = 84.66\%.$$

Table 6 shows detailed classification accuracies from comparisons of AMSR-E and FY3B-MWRI with the MODIS daily snow product (MYD10C1). From these comparisons, snow cover retrieved accuracy by the proposed passive microwave technique was 84%. AMSR-E snow cover accuracy was greater than FY3B-MWRI. This was because the AMSR-E scanning swath is larger than that of FY3B-MWRI, and its spatial resolution greater. Both factors affect snow cover accuracy. However, both AMSR-E and FY3B-MWRI can produce more accurate snow cover information than MODIS daily snow cover products.

5.4 Comparisons of retrieved snow depth and AMSR-E SWE products for China and entire northern hemisphere

SWE estimated using our algorithm for FY3B-MWRI was compared with that of the AMSR-E SWE product. AMSR-E covers the globe in 2 days, and FY3B-MWRI in 4–5 days. This results from their difference of observing swath. Therefore, AMSR-E and FY3B-MWRI brightness temperatures from 1–5 January 2011 were used for the comparison. Figure 7 compares their SWE estimates for the Northern Hemisphere. There are a total of 67706 pixels, and their SWE RMSE is 7.2 mm. Figure 8 shows the corresponding scatter plot, from which it is seen that AMSR-E overestimated SWE around China relative to FY3B-MWRI. This conclusion is consistent with other studies (Che et al., 2008; Sun, 2007; Savoie et al., 2009). Their difference is because they used different algorithms for the China area. Outside China, the FY3B-MWRI scheme used the same algorithm as that used by the AMSR-E team.

To expound the difference of these two algorithms in China, station snow depths from winter 2010–2011 were investigated. The observed data were from 89 days, between 1 December 2010 and 28 February 2011. Validation results are shown in Figures 7–9. Figure 8 shows error spatial distribution maps, using data from these two sensors across China during the aforementioned period. FY3B-MWRI snow depth inversion accuracy is superior to the AMSR-E standard snow depth products. The RMSE of FY3B-MWRI SWE is within 5 cm. However, those of AMSR-E products are clearly greater than those of the ground observations. Both algorithms exhibit larger errors in Northeast China, Xizang and northern Xinjiang than in central and northern regions of the country. This is because deep snow in China is usually found in the northeast, Xinjiang, and Xizang regions. Accuracies of FY3B-MWRI and AMSR-E algorithms are both lesser in forest and farmland regions. FY3B-MWRI estimation error is less than 10 cm in Northeast China, whereas RMSE of the AMSR-E standard snow depth product is greater than 20 cm. Larger errors of the FY3B-MWRI snow depth algorithm were in western China, such as the Jimunai, Fuyun, Aletai and Taicheng areas, which are around big cities. One reason is that urban emission characteristics are different from other land surfaces. The presence of cities in a grid cell strongly impacts the brightness temperature of the mixed pixel. The other reason is that stations in or near cities are not representative of satellite spatial grid values. Additionally, snow depth estimation error in areas bordering the Himalayas is large. Accuracies of the two algorithms are similar over grassland surfaces of the Xizang-Qinghai Plateau. In north-central China, both algorithms have good accuracy in grasslands of Inner Mongolia, but accuracy is poor in Gansu Province. It was found that stations there, such as Wuqiaoling and Menyuan, have shallow snow depths of 1–2 cm. Hence the poor performance of these algorithms re found in such areas.

Overall, the algorithm developed here is superior to that of AMSR-E. However, both had better performance in grassland than forest regions.

To investigate time series characteristics of the two algorithms in winter, snow depth between AMSR-E/FY3B-MWRI and station observations were compared over the period 1 December 2010 to 28 February 2011. Figure 9 presents the time series comparison. The black line is the RMSE time series of AMSR-E estimates, and the blue one is that from FY3B-MWRI; the red line is ground observation. The figure reveals that the algorithms have similar RMSE during the period, and that both agree with the ground observations. After 20 January 2010, the AMSR-E

Table 6 Error matrix calculated on comparisons between MODIS snow cover products and AMSR-E, FY3B-MWRI using the method developed in this work

	AMSR-E			FY3B-MWRI		
	Snow	No snow	Sum	Snow	No snow	Sum
MODIS snow cover	6006	1182	7188	4110	114	4224
MODIS snow free	43469	339023	382492	19978	106796	126774
Sum	49475	340205	389680	24088	106910	130998

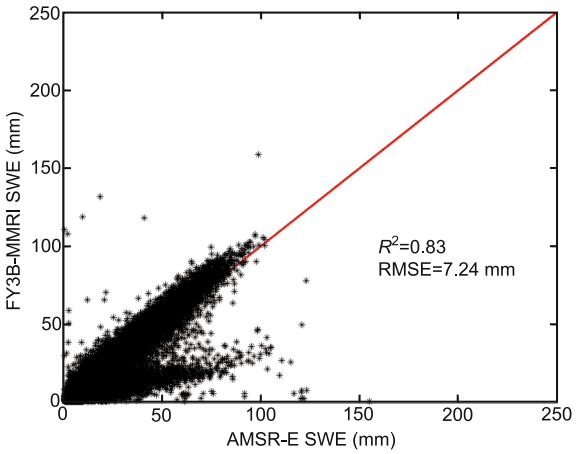

Figure 7 Comparison between FY3B-MWRI estimated snow depth and AMSR-E product in the north hemisphere.

method clearly overestimated snow depth relative to the ground observations. RMSE of FY3B-MWRI estimation is smaller than that of AMSR-E. RMSE of the algorithms are related to snow depth, i.e., RMSE increases with depth. This indicates that snow depth algorithms still have problems with deep snow cover, especially in forested areas.

6 Discussions and conclusions

The FY3 represents a new generation of polar-orbiting meteorological satellites. The MWRI aboard the FY3 platform is the first microwave radiometer on meteorological satellites. It can effectively monitor the land surface, atmosphere, and ocean. This work formulated snow depth algorithms for China with the FY3B-MWRI sensor configuration, using

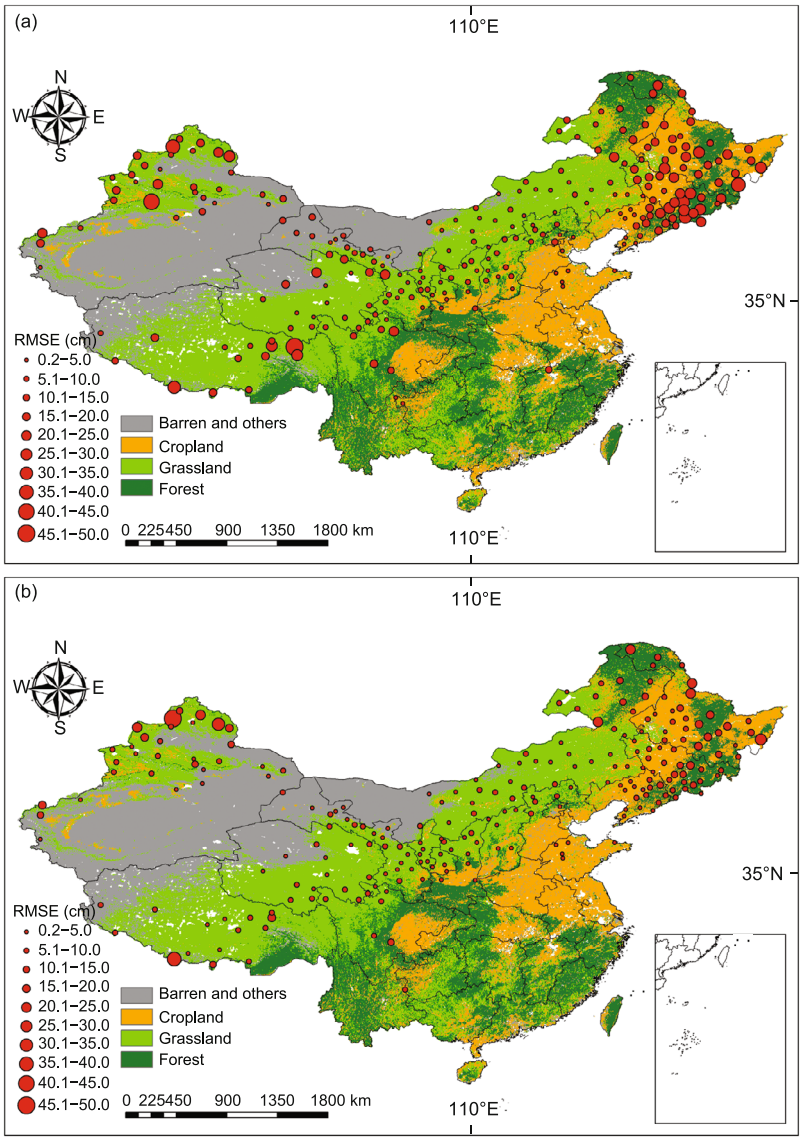

Figure 8 Satellite retrieved snow depth RMSE spatial distribution compared with ground snow depth from Dec. 1, 2010 to Feb. 28, 2011. (a) AMSR-E; (b) FY3B-MWRI.

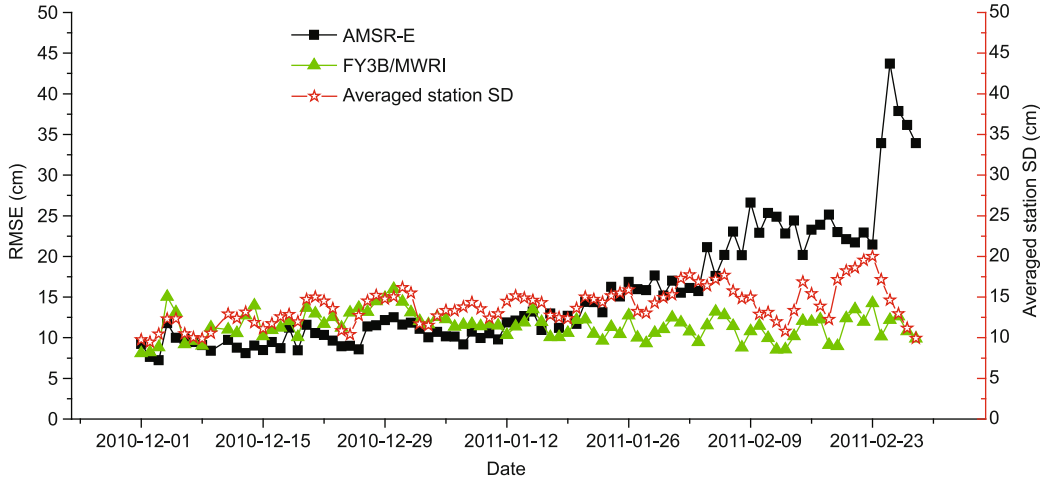

Figure 9 Time series snow depth RMSE of AMSR-E and FY3B-MWRI with the ground observation from Dec. 1, 2010 to Feb. 28, 2011. Black line: AMSR-E RMSE; blue line: FY3B-MWRI RMSE; red line: stations averaged snow depth.

7-year observations of AMSR-E and ground-based data. A linear decomposition technique of mixed pixels was used in development of the snow depth retrieval method. The LULC map contained 1-km fractional percentage data, and was used with FY3B-MWRI in an operational snow depth algorithm. In China, principal land cover types are grassland, farmland, bare ground, and forest. Based on spatial and temporal characteristics of snow depth, the high frequency of 89 GHz (sensitive to shallow snow) and low frequency of 10.7 GHz (sensitive to deep snow) were used in algorithm development for pure land cover types.

Snow depth estimated at satellite radiometer scale was summarized for different land surface types, by weighting the percentages of land cover types within each grid cell. Through validation with ground observations, the snow depth retrieval algorithms performed well for grassland and farmland surfaces. Snow-depth RMSE of grassland was only 2.74 cm, and that of farmland about 4.5 cm. However, performance was worst for forested areas, with underestimation of snow depth. Snow depths from both FY3B-MWRI and AMSR-E products were evaluated with ground measurements from winter 2011. The results show that FY3B-MWRI fared better than AMSR-E in China. Estimation accuracy of the former was lowest over forest-covered area with complex terrain, such as in Northeast China and North Xinjiang. This is because forest canopy weakens emission of snow at various frequencies. Forest emission increases with frequency. Sensitivity of the brightness temperature difference to snow depth is thereby reduced. Forest emission is a function of stem volume, forest closure, and canopy density. It is still unclear how to quantify these factors in algorithm inversion. Another potential reason is that forest areas in China are typically in mountainous regions. Both vegetation and rugged terrain pose great difficulties to accurate snow depth retrieval.

Wang et al. (2010) evaluated the effect of terrain on brightness temperature between 18.7 and 36.5 GHz frequencies, using Guo's algorithm (Guo et al., 2011). Their results show that terrain has less impact on snow depth using the brightness temperature difference at co-polarization. This difference at cross-polarization amplified terrain-induced errors in SWE inversion, by as much as 10 K. The errors were mainly in contiguous high-altitude mountain ranges such as the Altai, Qinghai-Tibet Plateau, and Rocky Mountains. Terrain correction was not done in our snow depth algorithm. The algorithms for both bare ground and forest used cross-polarization brightness temperature difference, which has some impacts on snow depth estimation for complex terrain. Thus, terrain effects for the operational snow depth algorithm require further study. This would aid the current algorithm for forested areas, by considering the effects of terrain, forest volume, closure and canopy density.

Furthermore, ground station data are not representative of average snow conditions within pixels of the passive microwave sensor. Moreover, because of rapid urbanization in China over the past three decades, meteorological stations are frequently located close to cities. Also, there are few stations on the Tibetan Plateau, with no observations at all in vast, unpopulated areas. This does not favor our method, which is based on semi-empirical regression relationships between ground-based data and satellite measurements. In addition, snow depth is shallow in most regions of China; 90% of all observations were of snow depth less than 20 cm. Therefore, the 89 GHz channel that is sensitive to shallow snow was incorporated in algorithm development. However, this frequency is affected by the atmosphere. It is necessary to do atmospheric correction at 36.5 and 89 GHz to improve inversion accuracy for snow depth. Some works (Tedesco et al., 2006; Wang et al., 2007) in the U.S. improved snow-covered area and SWE accuracy after correcting atmospheric effects at 18.7 and 36.5 GHz, using a radiative transfer model and atmospheric sounding data. More study is needed for applying current atmospheric correction techniques to the operational snow depth estimation algorithm.

Our approach depends only on satellite brightness temperature observation. Real-time snow depth monitoring will not only contribute to improvement of domestic passive microwave sensor instruments, but also to snow disaster monitoring. Snow depth monitoring in real-time is very important in decision making for disaster prevention and post-disaster reconstruction.

The authors would like to thank the Data Center for Resources and Environmental Sciences (RESDC), the Chinese Academy of Sciences (CAS) for the LULC map of China, the National Meteorological Information Center (NMIC) for the weather station data, and the National Snow and Ice Data Center (NSIDC) for the AMSR-E data. We are also grateful to the anonymous reviewers whose insightful comments have significantly improved the quality of this manuscript. This work was supported by the National Natural Science Foundation of China (Grant Nos. 41171260 & 41030534).

Cao M S, Li P J, Robinson D A, et al. 1993. Evaluation and primary application of microwave remote sensing SMMR derived snow cover in Western China. J Rem Sens, 8: 260–269

Chang A T C, Foster J L, Hall D K. 1987. Nimbus-7 SMMR derived global snow cover parameters. Ann Glaciol, 9: 39–44

Chang A T C, Gloersen P, Schmugge T J, et al. 1976. Microwave emission from snow and glacier ice. J Glaciol, 16: 23–29

Chang S, Shi J C, Jiang L M, et al. 2009. Improved snow depth retrieval algorithm in China area using passive microwave remote sensing data. In: Proceedings of 2009 IEEE International Geoscience and Remote Sensing Symposium. II: 614–617

Che T, Li X, Jin R, et al. 2008. Snow depth derived from passive microwave remote-sensing data in China. Ann Glaciol, 49: 145–154

Derksen C, Toose P, Rees A, et al. 2010. Development of a tundra-specific snow water equivalent retrieval algorithm for satellite passive microwave data. Remote Sens Environ, 114: 1699–1709

Derksen C, Walker A, Goodison B. 2005. Evaluation of passive microwave snow water equivalent retrievals across the boreal forest/tundra of western Canada. Remote Sens Environ, 96: 315–327

Derksen C. 2008. The contribution of AMSR-E 18.7 and 10.7 GHz measurements to improved boreal forest snow water equivalent retrievals. Remote Sens Environ, 112: 2701–2710

Foster J L, Chang A T C, Hall D K. 1997. Comparison of snow mass estimates from a prototype passive microwave snow algorithm, a revised algorithm and a snow depth climatology. Remote Sens Environ, 62: 132–142

Foster J L, Hall D K, Chang A T C, et al. 1984. An overview of passive microwave snow research and results. Rev Geophys Space Phys, 22: 195–208

Goïta K, Walker A, Goodison B. 2003. Algorithm development for the estimation of snow water equivalent in the boreal forest using passive microwave data. Int J Remote Sens, 24: 1097–1102

Grody N C, Basist A N. 1996. Global identification of snowcover using SSM/I measurements. IEEE Trans Geosci Remote Sens, 34: 237–249

Grody N C. 1991. Classification of snow cover and precipitation using the special sensor microwave imager. J Geophys Res, 96: 7423–7435

Guo Y, Shi J, Du J, et al. 2011. A topographic correction technique for satellite radiometer measurement with high resolution DEM. Int J Remote Sens, 32: 8899–8913

Hallikainen M T, Jolma P. 1992. Comparison of algorithms for retrieval of snow water equivalent from Nimbus-7 SMMR data in Finland. IEEE Trans Geosci Remote Sens, 30: 124–131

Hofer R, Mätzler C. 1980. Investigation of snow parameters by radiometry in the 3- to 60-mm wavelength region. J Geophys Res, 85: 453–460

Kelly R E J. 2009. The AMSR-E snow depth algorithm: Description and initial results. J Remote Sens Soc Japan, 29: 307–317

Koenig L S, Forster R R. 2004. Evaluation of passive microwave snow water equivalent algorithms in the depth hoar-dominated snowpack of the Kuparuk River Watershed, Alaska, USA. Remote Sens Environ, 93: 511–527

Liston E G. 2004. Representing subgrid snow cover heterogeneities in regional and global models. J Climate, 17: 1381–1397

Li X J, Liu Y J, Zhu X X, et al. 2007. Snow cover identification with SSM/I data in China. J Appl Meteor Sci, 18: 12–20

Rott H, Sturm K. 1991. Microwave signature measurements of Antarctic and Alpine snow. Proceedings of the 11th EARSeL Symposium, European Association of Remote Sensing Laboratories in Boulogne-Billancourt. 140–151

Savoie M H, Armstrong R L, Brodzik M J, et al. 2009. Atmospheric corrections for improved satellite passive microwave snow cover retrievals over the Tibet Plateau. Remote Sens Environ, 113: 2661–2669

Shuman C, Alley R. 1993. Spatial and temporal characterization of hoar formation in central Greenland using SSM/I brightness temperatures. Geophys Res Lett, 20: 2643–2646

Singh P R, Gan T Y. 2000. Retrieval of snow water equivalent using passive microwave brightness temperature data. Remote Sens Environ, 74: 275–286

Sun Z W. 2007. Estimate snow depth and snow water equivalent algorithm for FY-3 MWRI and development of system. Master Thesis. Beijing: Beijing Normal University

Tait A B. 1998. Estimation of snow water equivalent using passive microwave radiation data. Remote Sens Environ, 64: 286–291

Tedesco M, Wang J R. 2006. Atmospheric correction of AMSR-E brightness temperatures for dry snow cover mapping. IEEE Trans Geosci Remote Sens Lett, 3: 320–324

Ulaby F T, Moore R K, Fung A. 1981. Microwave remote sensing: Active and passive, vol. 1: Microwave remote sensing fundamentals and radiometry. Reading, Massachusetts: Addison-Wesley-Longman. 456

Wang J R, Tedesco M. 2007. Identification of atmospheric influences on the estimation of snow water equivalent from AMSR-E measurements. Remote Sens Environ, 111: 398–408

Wang P, Jiang L, Zhang L, et al. 2010. Impact of terrain topography on retrieval of snow water equivalence using passive microwave remote sensing. In: Proceedings of 2010 IEEE International Geoscience and Remote Sensing Symposium. 1757–1760

Wu T W, Wu G X. 2004. An empirical formula to compute snow cover fraction in GCMs. Adv Atmosph Sci, 21: 529–535

Yang H, Weng F Z, Lv L Q, et al. 2011a. The FengYun-3 microwave radiation imager on-orbit verification. IEEE Trans Geosci Remote Sens, 49: 4552–4560

Yang H, Lv L Q, Xu H X, et al. 2011b. Evaluation of FY3B-MWRI instrument on-orbit calibration accuracy. In: Proceedings of 2011 IEEE International Geoscience and Remote Sensing Symposium. 2252–2254